Flying Focus and Its Application to Plasma-Based Laser Amplifiers

D. Turnbull, S.-W. Bahk, I. A. Begishev, R. Boni, J. Bromage, S. Bucht, A. Davies, P. Franke, D. Haberberger, J. Katz, T. J. Kessler, A. L. Milder, J. P. Palastro, J. L. Shaw, D. H. Froula

University of Rochester Laboratory for Laser Energetics, 250 E River Rd., Rochester, NY 14623, USA

E-mail: `turnbull@lle.rochester.edu`

Abstract. Combining a chirped laser pulse with a chromatic lens yields a flying focus—a laser focus that moves dynamically in time. This provides control over the propagation of the peak laser intensity within an extended focal region that can be many times larger than the system's Rayleigh length. Any velocity is achievable, including backward relative to the laser propagation direction. Previous simulation results have shown that a laser beam with a flying focus can create a counter-propagating ionization wave and subsequently pump a frequency-downshifted laser via the stimulated Raman scattering instability. Compared to a conventional Raman amplification scheme, several advantages were highlighted, including improved temperature control, plasma uniformity, and precursor growth mitigation. Here, we extend those results to demonstrate additional benefits: (1) the flying focus makes it possible for an *unseeded* Raman amplifier to produce a short, high-intensity beam; and (2) the flying focus minimizes collisional absorption of the pump, facilitating amplifier operation at higher plasma densities. Preliminary experiments have laid the groundwork for a high-performance plasma-based laser amplifier. The focal spot dynamics were initially confirmed at low intensity. It was subsequently demonstrated that ionization waves of arbitrary velocity can be produced at higher intensity. Here, we show a counter-propagating ionization front moving at approximately the speed of light—the optimal result for a Raman amplifier.

1. Introduction

The development of plasma-based laser amplifiers is motivated by the desire for a compact laser system that can reach unprecedented laser intensities. The idea is to use stimulated scattering in plasma—either the Raman [1, 2, 3, 4] or the Brillouin [5, 6, 7, 8] instability—to transfer energy from a relatively long laser pulse to an ultrashort laser pulse that reaches much higher intensity. Raman amplification experiments usually consist of the following components: a preformed plasma with uniform density over length l (often produced using one or more separate laser systems), an energetic "pump" laser beam with a temporal duration of at least $2l/c$, and an ultrashort "seed" pulse

that is frequency downshifted to satisfy a resonant matching condition with the pump and electron plasma wave [9, 10, 3, 11, 12, 13, 14].

These experiments have failed to perform according to theoretical predictions, despite attempting to operate in an optimal parameter space constrained by collisional absorption, Landau damping, wavebreaking, and other effects [15, 16]. One challenge that is often highlighted is the production of uniform preformed plasma channels satisfying the resonance condition over several millimeters [9, 10, 17]. Another difficulty is creating a seed pulse with the appropriate frequency shift that is energetic enough to quickly enter the nonlinear pump-depletion regime. Several additional complications arise from the pump's traversal of the plasma prior to meeting the seed, including precursor stimulated scattering signals that grow from noise [2, 18, 14] and undue levels of plasma heating resulting in excessive Landau damping and/or detuning from the Bohm–Gross frequency shift or kinetic nonlinear frequency shifts [19, 17, 11, 20, 21].

Several schemes have been proposed to eliminate individual ingredients of a plasma-based amplifier. For example, seed-ionized amplifiers were proposed to avoid the need for the creation of, and pump passage through, a preformed plasma [22, 23]. This scheme, however, places undue requirements on the initial seed pulse. More recent theoretical work showed that equivalent amplifier performance can be obtained if a plasma wave seed replaces the frequency-shifted laser seed pulse [24]; however, the capacity to engineer a plasma wave seed remains to be seen.

Turnbull *et al.* [25] were the first to propose using a "flying focus" [26, 27] in a plasma amplifier. By synchronizing the pump's spot size and intensity to the seed pulse propagation, it was shown in simulations that the plasma could be produced dynamically by the pump just prior to the seed's arrival. Issues related to the pump's propagation through plasma are eliminated because the pump propagates primarily through gas. Reference [25] considered a 1ω (1.054 μm wavelength) pump at a fairly low plasma density ($n_e = 6 \times 10^{18}$ cm^{-3}), a regime in which the main advantages provided by the flying focus were temperature control and suppression of precursor growth ahead of the seed. Here, we extend those results in several ways: The first extension is simply turning off the seed but allowing growth from noise. It is observed that a single short pulse in time grows within the window that would otherwise have been occupied by the seed. It may therefore be possible to eliminate the injected seed altogether; together with eliminating the preformed plasma, this greatly simplifies a Raman plasma amplifier and may improve the odds of a successful experimental implementation. The second extension is to consider a 2ω pump at an order-of-magnitude higher density ($n_e = 6{\times}10^{19}$ cm^{-3}). In that case, we see that collisional absorption of the pump while propagating a long distance through the higher density plasma is another limitation of conventional focusing that is mitigated by the dynamic ionization wave. In addition to these new simulations, we also review preliminary flying focus experiments that lay the groundwork for a high-performance flying focus Raman amplifier.

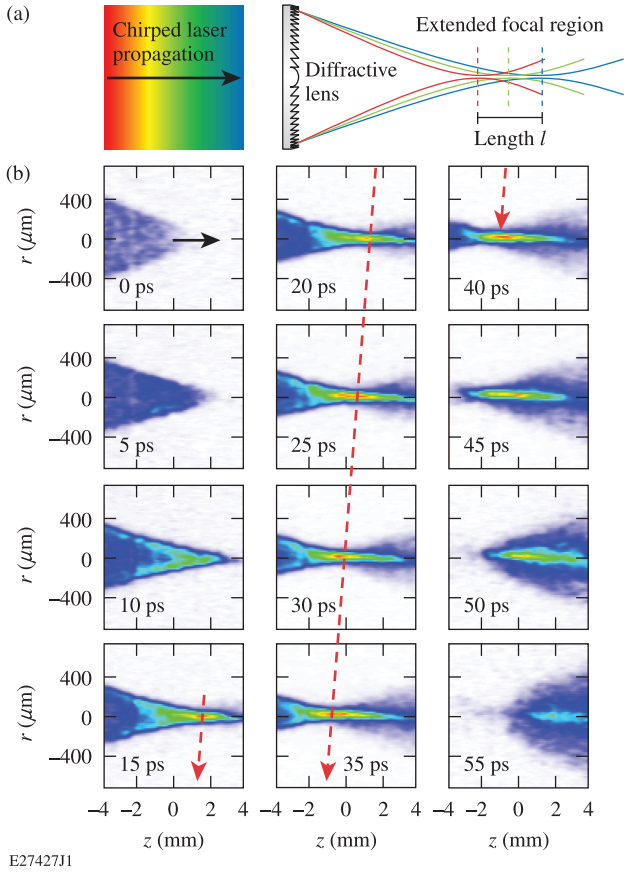

Figure 1. Example of a flying focus. (a) When a diffractive lens linearly disperses the focal positions within a laser's bandwidth over a distance l, and the laser is negatively chirped with duration $2l/c$, the focus will move backward at the speed of light between the times at which the blue and red ends of the spectrum arrive at best focus. (b) Experimental data are shown for a similar case of backward focal spot motion (in this case slower than the speed of light because of the longer pulse length that was used).

2. Flying Focus

When a linearly chirped laser pulse with duration τ (with the sign of τ indicating the direction of the chirp) is focused by a diffractive lens providing linear chromatic dispersion of the laser focus over a distance l, the focal spot moves at a velocity that is uniquely determined by the ratio τ/l. Consider the intuitive example (and the one most relevant to a plasma amplifier) illustrated in Fig. 1(a) in which $\tau = -2l/c$. The shortest wavelength will be the first to arrive at best focus at the exit of the focal region. All colors subsequently pass through their own respective focal spots over a time period $\Delta t = l/c$, finishing with the red side of the spectrum at the entrance to the focal region. Since it takes a time l/c for the focus to move a distance $-l$, the focal-spot velocity is $v_f = -c$. The more general velocity derivation can be found in other references [26, 27, 28, 29].

The expected motion of the focal spot was confirmed experimentally in Ref. [26]; we

reproduce a relevant example here. In the experiment, a diffractive lens with $f_0 = 51.1$ cm focused low intensity laser light in an $f/7$ geometry in air, creating an extended focal region. This focus was imaged onto the entrance slit of an ultrafast streak camera with a 7 ps instrument response function, yielding temporally resolved 1-D images of the laser focus at a given point in space. Keeping the pulse duration fixed, the imaging lens was translated along the laser axis in increments of Δz to image different locations within, before, and after the focal region.

Each of these original images represented the laser focal spot at a single point in space but every point in time. To view the data as a movie of the laser pulse propagating through space, each image was divided into temporal slices $\Delta t = \Delta z/c$ that were regrouped to create frames representing a single point in time but every measured point in space. Figure 1(b) shows 12 frames at 5 ps intervals for a data set where the full width at half maximum (FWHM) pulse duration and spectral bandwidth were $\tau = -52$ ps and $\Delta\lambda = 8.7$ nm, respectively. Since $l = f_0\Delta\lambda/\lambda_0$ with the diffractive lens, $\tau \approx -3.5l/c$ in this case (longer than the $-2l/c$ case just described) and the focus still moves backward but slower than the speed of light; $v_f/c = -0.51$ was measured using the technique described in Ref. [26]. Note also that the streak camera limited the spatial resolution to ≈ 50 μm, so best focus (≈ 15 μm FWHM) is poorly resolved. This narrowed the dynamic range in a way that was beneficial for measuring lower intensity light away from best focus, but it failed to capture the degree to which the peak laser intensity is localized to, and travels with, the location of best focus.

Nevertheless, the data illustrate the salient physics. The leading edge (blue end of the spectrum) converges to best focus at around $z = +2$ mm along the laser axis. Subsequently, the location of best focus moves backward at a constant rate as other colors converge to their own respective focal spots, finishing with the red end of the spectrum near $z = -2$ mm. Showing frames before and after any portion of the spectrum is at best focus clarifies the fact that the wave packet is propagating to the right at the group velocity of light in the medium, as expected. Laser intensity is maximized, however, when the laser spot size in minimized, so peak laser intensity will dynamically track the moving focus. Away from best focus in the quasi-far field, lower intensity isosurfaces will move at approximately the same velocity. Therefore, an optimal intensity for a given application can be selected by appropriate displacement of a region of interest from the region of best focus.

3. Three-wave modeling of Raman amplification

Reference [25] began to investigate the impact of the flying focus on a Raman amplifier using the common three-wave modeling framework (see, e.g., Refs. [23] and [15] and references therein). We briefly reintroduce the model here. Neglecting plasma wave

advection and the possibility of frequency detuning, the basic three-wave equations are

$$\begin{aligned}(\partial_t - v_1\partial_x + \nu_1)\, a_1 &= K a_2 a_3,\\ (\partial_t - v_2\partial_x + \nu_2)\, a_2 &= -K a_1 a_3^*,\\ (\partial_t + \nu_3)\, a_3 &= -K a_1 a_2^* + S_3,\end{aligned} \tag{1}$$

where the subscripts 1, 2, and 3 refer to the pump, the seed, and the electron plasma wave (EPW), respectively; v_i's are group velocities; ν_i's are damping rates; $K = \omega(n_e/n_c)^{1/4}/2$ is the wave coupling parameter, where n_e is the electron density and n_c is the critical density; $a_{1,2} = 0.855\times10^{-5}\lambda_{1,2}[cm]\sqrt{I_{1,2}[W/cm^2]}$ are normalized laser vector potentials, and $a_3 = |e|\,\langle E_3\rangle\,/m_e c\sqrt{\omega\omega_{pe}}$ is the normalized envelope of the EPW, with pump frequency ω and EPW frequency ω_{pe}. The pump and seed are damped collisionally, $\nu_{1,2} = \nu_{ei}\frac{\omega_{pe}^2}{\omega^2}$ where $\nu_{ei} = 2.9\times10^{-6}Zn_e[cm^{-3}]\Lambda T_e[eV]^{-3/2}$ and Λ is the Coulomb logarithm; $\nu_3 = \nu_{ei} + \nu_l$ includes both collisional absorption and collisionless (Landau) damping for the EPW, with $\nu_l \approx \sqrt{\frac{\pi}{2}}\frac{\omega_{pe}^4}{(k_3 v_e)^3}\exp\left[\frac{-\omega_{pe}^2}{2(k_3v_e)^2}\right]$. S_3 is a noise term that is included to investigate spontaneous stimulated Raman scattering (SRS) growing from undriven plasma fluctuations. Following Ref. [15], thermal noise is given by $\langle S_3(x,t)S_3(x',t')\rangle = \Sigma_3\delta(x-x')\delta(t-t')$, where $\Sigma_3 = \frac{\omega}{2\pi}\frac{k_3^2}{n_c}\frac{\nu_3}{\omega_{pe}}\frac{T_e}{m_e c^2}$ and $\langle ...\rangle$ represents an ensemble average.

In addition to the coupled wave equations describing the evolution of the pump, seed, and electron plasma wave, an ionization model was included to simulate plasma formation by the pump[23]:

$$\begin{aligned}\partial_t n_e &= n_n w(a_1),\\ \partial_t n_n &= -n_n w(a_1),\end{aligned} \tag{2}$$

where n_n is the neutral gas density and $w(a_1)$ is the ionization rate that depends on the local pump intensity. In the regime of interest, the Keldysh formula is valid [30, 31]. For $\gamma = \sqrt{2U_I/m_e c^2}/a_1 \gg 1$, where U_I is the ionization potential, the multiphoton ionization rate $w(a) \cong \omega N^{3/2}\,(2\gamma)^{-2N}$ is appropriate, where $N = 1 + Int(U_I/\hbar\omega)$ is the number of photons required to overcome the ionization potential. For $\gamma \ll 1$, the tunneling formula is more accurate:
$w(a) \cong 4\Omega_0\left(\frac{U_I}{U_H}\right)^{5/2}\frac{a_H}{a_1}\exp\left[-\frac{2}{3}\left(\frac{U_I}{U_H}\right)^{3/2}\frac{a_H}{a_1}\right]$, with atomic frequency $\Omega_0 \cong 4.1\times10^{16}$ s^{-1}, hydrogen ionization potential $U_H = 13.6$ eV, and the hydrogenic electric field normalized vector potential $a_H \cong 3.05\times10^{14}/\omega$. An exponential fit was used to fill in the region between the multiphoton and tunneling regimes. The molecular nature of hydrogen was approximated by using the molecular ionization potential $U_I = U_{H_2} = 15.4$ eV [23]. To conserve energy, an additional damping term on the pump was added to Eq. (1) by balancing the equation, $n_c\frac{m_e c^2}{2}\partial_t a_1^2 = -(U_I+\epsilon)\partial_t n_e$, where $\epsilon = m_e v_{osc}^2/2$ is the assumed birth energy and v_{osc} is the oscillation velocity of electrons in the pump laser's electric field. The electron temperature was initialized locally at the birth energy, but it can subsequently evolve to balance collisional absorption of the pump and seed as well as flux-limited thermal transport.

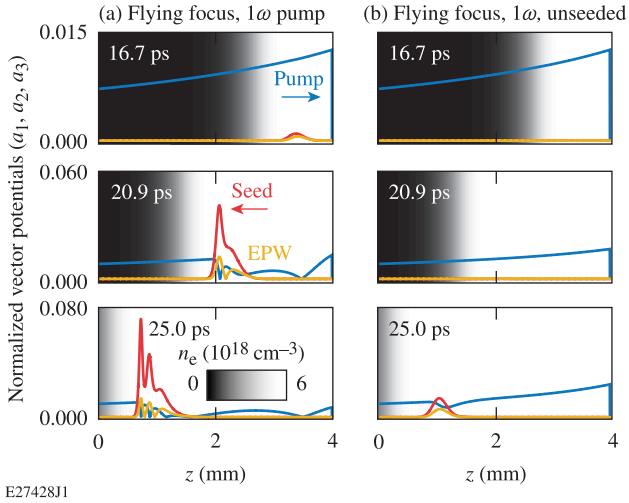

Figure 2. Three-wave modeling results of seeded and unseeded plasma amplifiers using a flying focus. (a) Ideal performance is observed with a 1ω pump and $n_e = 6 \times 10^{18}$ W/cm^2 plasma density. The seed is injected just behind the ionization front and encounters more or less constant plasma conditions along its entire path. (b) Without injecting a seed, Raman scattering grows from thermal noise but still evolves into a single pulse that is short in duration because the optimal window for amplification is narrow. Given additional length over which to grow, this signal will also reach the pump-depletion stage, raising the possibility of a high-performance unseeded amplifier.

The interaction length was 4 mm in all simulations, defining a pump duration of 26.7 ps. For seeded simulations, a 500-fs–duration FWHM seed pulse with an initial intensity $I = 10^9$ W/cm^2 was injected at the right edge just after the arrival of the pump's leading edge ($t = 14$ ps). The pump was specified by its focusing geometry ($f/12$) as well as its spot diameter (500 μm) and intensity at the location of the injected seed pulse. The pump was assumed to remain in converging space, with best focus located behind the injected seed pulse, but the pump intensity was evolved according to geometric optics and a focus that moves backward at $v_f = -c$.

Keeping with the very similar examples shown in Ref. [25], Fig. 2 features a 1ω ($\lambda = 1$ μm) pump with an intensity (at the seed location) of $I = 1.6 \times 10^{14}$ W/cm^2. The first frame in each case clearly shows the pump intensity increasing along z as the pump converges toward best focus. Since the ionization threshold of the $n_n = 6 \times 10^{18}$ cm^{-3} background hydrogen gas ($\approx 10^{14}$ W/cm^2) is first exceeded at the right edge of the simulation volume, plasma is initialized there and an ionization front propagates to the left at the speed of the flying focus. Since the flying focus is deliberately synchronized to the seed pulse, the ionization front propagates just ahead of the injected seed beam.

Two advantages of this dynamic ionization front were highlighted in Ref. [25]: (1) the limited extent of plasma ahead of the seed pulse prevents spontaneous SRS, which is known to compete with the desirable seed amplification; and (2) the fixed but tunable duration of the plasma's existence prior to the seed's arrival at every point throughout the interaction region allows the electron temperature to be optimized, balancing effects

such as collisional damping, Landau damping, particle trapping, and wavebreaking.

Figure 2(b) highlights an additional advantage— the possibility of growing a short, high-intensity seed from thermal noise. The only difference between the simulations in Figs. 2(a) and 2(b) is that no seed was injected in the latter case. While no scattered light is visible in the first two frames, a signal is seen to be approaching the pump-depletion regime by the third frame. This pulse occupies the same window into which the seed was previously injected. The key highlight here is the self-organization of a signal that grows from random thermal noise into a single short pulse, which is unusual for spontaneous signals. It is particularly surprising to see the finite duration of the back end of the signal, because when the pump is not rapidly depleted by transferring energy to the seed, it continues to converge, reaching even higher intensities. The effect of the higher pump intensity appears to be outweighed, however, by the rapidly increasing electron temperature and associated Landau damping. Therefore, there is a narrow traveling window within which the growth of Raman scattering is favored, resulting in the aforementioned self-organization. Noting the change in scale of the y axis, the thermal signal in the third frame of Fig. 2(b) is much larger than the injected signal in the first frame of Fig. 2(a). Therefore, an additional ≈ 2 mm of propagation may be enough to compensate for the lack of an injected seed.

While the maximum possible energy transfer efficiency in an unseeded case would obviously be limited by the fact that at least the first ≈ 10 ps of the pump will likely not be depleted, this might be deemed an acceptable tradeoff given the compelling advantages of this scheme. As previously mentioned, experiments have been challenged by the need to produce long, uniform plasmas along with a resonant frequency-shifted seed pulse. In this case, as long as the background gas density is uniform (likely easier to ensure than a uniform preformed plasma), the self-similar nature of the ionization front ensures the plasma conditions are constant in a frame moving with the growing signal. Also in the case of growth from thermal noise, the signal will automatically be resonant with the resulting plasma. By eliminating the complexity introduced by both the preformed plasma *and* the injected seed pulse, this system's performance may get closer to what the theory predicts.

Figure 3 considers a somewhat different regime with a 2ω ($\lambda = 0.5$ μm) pump and order of magnitude higher ($n_n = 6 \times 10^{19}$ cm^{-3}) initial gas density. Figure 3(a) shows the standard simulation including the flying focus, with excellent amplifier performance similar to Fig. 2(a). When the pump beam is instead assumed to be collimated while crossing the focal region (prescribing the spot size and intensity at the left edge instead of at the peak of the injected seed), the leading edge of the pump burns through the gas as it propagates across the interaction region, losing significant energy to both ionization and collisional absorption [note the decaying pump intensity in the first frame of Fig. 3(b)]. Growth in that case is further limited by the fact that the plasma remains partially ionized by the time the seed starts to enter the interaction region, as well as the fact that excessive plasma heating by the pump limits seed growth due to Landau damping. We see in Fig. 3(c) that artificially fixing the electron temperature seen by the seed

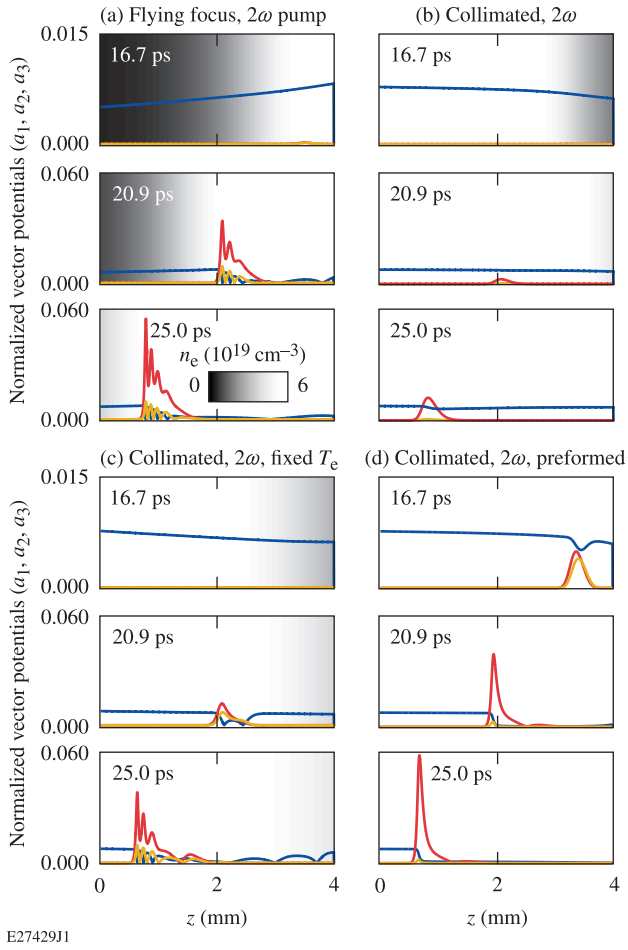

Figure 3. Additional three-wave modeling results for a 2ω pump and higher plasma density. (a) Similar ideal performance is observed with a flying focus. (b) Given the equivalent pump intensity and plasma density but no flying focus, performance is much poorer due the pump energy losses to ionization and collisional absorption as well as higher Landau damping due to elevated plasma temperatures. (c) Artificially fixing the electron temperature to be similar to the flying focus example restores much but not all of the growth. (d) Similarly, preforming the plasma restores strong growth in these simulations. However, noise was turned off in these 2ω pump simulations, and in reality, a preformed plasma would be very unstable to premature Raman scattering at this high density.

pulse to be similar to the flying focus example in Fig. 3(a) recovers much but not all of the seed growth.

Although a uniform preformed plasma would restore strong seed growth even in the case of a collimated pump that is subject to collisional absorption and strongly heats the plasma during its propagation [as shown in Fig. 3(d)], note that this is true only because noise has been turned off in these 2ω simulations. Otherwise, all of these higher density, 2ω pump simulations are very unstable to precursor growth. Given the way that noise is treated in these simulations, spontaneous signals (if allowed) would even degrade the case of Fig. 3(a) because thermal signals would grow along the density ramp

of the ionization front. However, a more rigorous calculation should include the effect of "photon acceleration" [32, 33] resulting from the moving refractive index gradient, which would be expected to detune such thermal signals before they can reach levels at which they compete with the seed amplification.

4. Ionization waves of arbitrary velocity

After demonstrating the expected focal spot motion at low intensity, the next step was to demonstrate the ability to produce ionization waves of arbitrary velocity (IWAV's), including the $v_f = -c$ case that is ideal for a plasma-based laser amplifier. This second experiment used the same laser ($\Delta\lambda = 8.7$ nm) and diffractive lens ($f/7$, $f_0 = 51.1$ cm) described earlier, but increasing the energy in each pulse up to ≈ 25 mJ produced intensities in the low- to mid-10^{14} W/cm^2 range at best focus—sufficient to produce a spark in ambient air. The IWAV tracked the velocity of best focus, as predicted by Palastro *et al.* [28]. The plasma channel dynamics were diagnosed using spectrally resolved 1-D schlieren of a chirped 2ω probe beam. The probe beam's linear chirp equated spectral resolution with temporal resolution, so the diagnostic effectively captured the existence of sharp plasma gradients transverse to the z axis (i.e., the edge of the channel) as a function of time [Fig. 4(a)].

The IWAV velocities were determined by fitting a straight line through the points identified by an edge-finding routine. Several results were presented in Ref. [29]. In Fig. 4(b), we show a case where the pump (and probe) pulse duration was $\tau = -31$ ps ($\approx -2l/c$), resulting in an ionization front traveling backward at approximately the speed of light [$v_f = (-2.8 \pm 0.4) \times 10^8$ m/s]. This is the ideal case for a plasma-based laser amplifier.

In Refs. [28] and [29], it was emphasized that superluminal and/or backward IWAV propagation mitigates the issue of ionization-induced refraction that typically inhibits the formation of long, contiguous plasma channels. Figure 4(c) reproduces the case in which the pump has positive chirp ($\tau = +20$ ps), yielding a subluminal forward propagating flying focus. Since the photons reaching larger values along the z axis have to (attempt to) propagate through plasma formed earlier by the red side of the spectrum, ionization-induced refraction produces losses that ultimately result in a disjointed plasma channel. This issue was neglected in the plasma amplifier simulations that assumed a collimated pump beam [Figs. 3(b)–3(d)]. Therefore, attempting to use a conventional focusing geometry on a plasma-forming pump beam would likely result in even poorer performance than those simulations would suggest.

5. Summary and future work

In conclusion, the use of a flying focus will greatly improve the performance of a plasma-based laser amplifier in which the pump is also the plasma-forming beam. Several of the advantages provided by the flying focus are captured by simple three-wave model

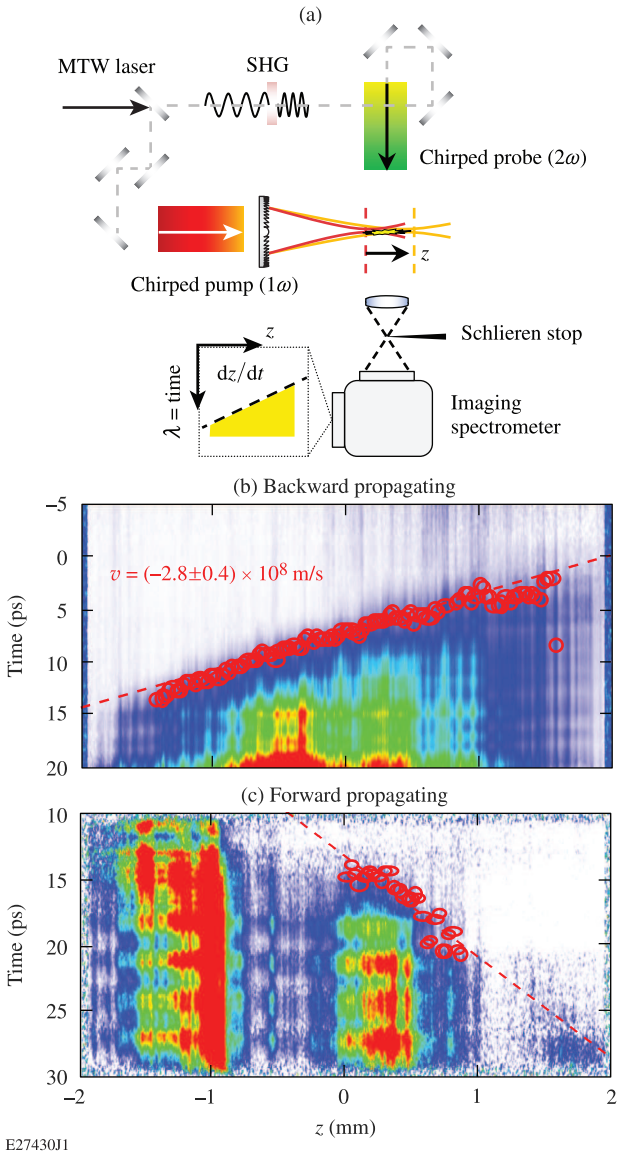

Figure 4. Ionization wave of arbitrary velocity (IWAV) experimental setup and results. (a) An energetic chirped pump beam was focused by a diffractive lens, reaching intensities above the ionization threshold of ambient air at best focus, which produced an ionization front that traveled at the velocity of the flying focus. The IWAV was diagnosed using spectrally-resolved schlieren of a chirped probe beam. Spectral resolution translates to temporal resolution by exploiting the linear time-frequency relationship of the chirped probe beam. (b) The data showed an IWAV moving backward at the speed of light (within error bars) when $\tau \approx -2l/c$. (c) When the pump was positively chirped (resulting in a subluminal forward-propagating focus), ionization-induced refraction compromised the plasma channel formation.

simulations, including the minimization of pump collisional absorption (facilitating higher density amplifiers than might otherwise be possible) and optimization of plasma temperature. The new simulations here also highlight the possibility that an unseeded Raman amplifier can still produce a short pulse beam that reaches the pump-depletion regime. By eliminating the complexities introduced by both the preformed plasma and the carefully engineered seed pulse, this scheme may greatly increase the odds of a successful experimental implementation. As preliminary steps toward this end goal, we first verified the expected dynamics of the flying focus. We subsequently demonstrated the ability to produce ionization waves that follow the laser focus, here highlighting the desirable case for plasma-based laser amplifiers in which the IWAV propagates at $v_f \approx -c$.

In the future, it will be necessary to demonstrate that larger diameter plasma channels can be produced while preserving the beneficial dynamics that we have observed at best focus. Since the pump intensity is constrained in an optimized Raman amplifier and the output seed intensity is generally assumed to be limited (at best) by relativistic effects, plasma amplifiers capable of reaching truly unprecedented intensities are thought to be possible only by increasing the beam diameters in tandem with the available pump energy and then focusing the resulting amplified seed. For this reason, the simulations above assume that the pump remains in the quasi-far field within the interaction region, with a fairly large spot size at the location of the injected seed beam. Whether we can ionize a larger volume away from best focus remains to be seen. Similarly, once a given color reaches the ionization threshold of the background gas, we know that ionization-induced refraction may act to defocus that color, so it must be demonstrated that each color remains localized long enough to pump the injected seed pulse (or the thermal noise that resides in the optimal window of amplification).

This work was supported by the U.S. Department of Energy Office of Fusion Energy Sciences under contract No. DE-SC0016253, Department of Energy under Cooperative Agreement No. DE-NA0001944, the University of Rochester, and the New York State Energy Research and Development Authority. The support of DOE does not constitute an endorsement by DOE of the views expressed in this article.

References

[1] Malkin V M, Shvets G and Fisch N J 1999 *Phys. Rev. Lett.* **82**(22) 4448–4451
[2] Malkin V M, Shvets G and Fisch N J 2000 *Phys. Rev. Lett.* **84**(6) 1208–1211
[3] Ren J, Cheng W, Li S and Suckewer S 2007 *Nat. Phys.* **3** 732–736 ISSN 1745-2473
[4] Trines R M G M, Fiuza F, Bingham R, Fonseca R A, Silva L O, Cairns R A and Norreys P A 2011 *Nat. Phys.* **7** 87–92 ISSN 1745-2473
[5] Andreev A A, Riconda C, Tikhonchuk V T and Weber S 2006 *Phys. Plasmas* **13** 053110 ISSN 1070-664X
[6] Lancia L, Marquès J R, Nakatsutsumi M, Riconda C, Weber S, Hüller S, Mančić A, Antici P, Tikhonchuk V T, Héron A, Audebert P and Fuchs J 2010 *Phys. Rev. Lett.* **104**(2) 025001
[7] Lehmann G and Spatschek K H 2013 *Phys. Plasmas* **20** 073112 ISSN 1070-664X

[8] Weber S, Riconda C, Lancia L, Marquès J R, Mourou G A and Fuchs J 2013 *Phys. Rev. Lett.* **111**(5) 055004
[9] Ping Y, Cheng W, Suckewer S, Clark D S and Fisch N J 2004 *Phys. Rev. Lett.* **92**(17) 175007
[10] Cheng W, Avitzour Y, Ping Y, Suckewer S, Fisch N J, Hur M S and Wurtele J S 2005 *Phys. Rev. Lett.* **94**(4) 045003
[11] Ping Y, Kirkwood R K, Wang T L, Clark D S, Wilks S C, Meezan N, Berger R L, Wurtele J, Fisch N J, Malkin V M, Valeo E J, Martins S F and Joshi C 2009 *Phys. Plasmas* **16** 123113 ISSN 1070-664X
[12] Turnbull D, Li S, Morozov A and Suckewer S 2012 *Phys. Plasmas* **19** 073103 ISSN 1070-664X
[13] Turnbull D, Li S, Morozov A and Suckewer S 2012 *Phys. Plasmas* **19** 083109 ISSN 1070-664X
[14] Vieux G, Cipiccia S, Grant D W, Lemos N, Grant P, Ciocarlan C, Ersfeld B, Hur M S, Lepipas P, Manahan G G, Raj G, Gil D R, Subiel A, Welsh G H, Wiggins S M, Yoffe S R, Farmer J P, Aniculaesei C, Brunetti E, Yang X, Heathcote R, Nersisyan G, Lewis C L S, Pukhov A, Dias J M and Jaroszynski D A 2017 *Sci. Rep.* **7** 2399 ISSN 2045-2322
[15] Clark D S and Fisch N J 2003 *Phys. Plasmas* **10** 3363–3370 ISSN 1070-664X
[16] Sadler J D, Trines R M G M, Tabak M, Haberberger D, Froula D H, Davies A S, Bucht S, Silva L O, Alves E P, Fiúza F, Ceurvorst L, Ratan N, Kasim M F, Bingham R and Norreys P A 2017 *Phys. Rev. E* **95**(5) 053211
[17] Pai C H, Lin M W, Ha L C, Huang S T, Tsou Y C, Chu H H, Lin J Y, Wang J and Chen S Y 2008 *Phys. Rev. Lett.* **101**(6) 065005
[18] Tsidulko Y A, Malkin V M and Fisch N J 2002 *Phys. Rev. Lett.* **88**(23) 235004
[19] Berger R L, Clark D S, Solodov A A, Valeo E J and Fisch N J 2004 *Phys. Plasmas* **11** 1931–1937 ISSN 1070-664X
[20] Farmer J P, Ersfeld B and Jaroszynski D A 2010 *Phys. Plasmas* **17** 113301 ISSN 1070-664X
[21] Yang X, Vieux G, Brunetti E, Ersfeld B, Farmer J P, Hur M S, Issac R C, Raj G, Wiggins S M, Welsh G H, Yoffe S R and Jaroszynski D A 2015 *Sci. Rep.* **5** 13333 ISSN 2045-2322
[22] Malkin V M and Fisch N J 2001 *Phys. Plasmas* **8** 4698–4699
[23] Clark D S and Fisch N J 2002 *Phys. Plasmas* **9** 2772–2780 ISSN 1070-664X
[24] Qu K, Barth I and Fisch N J 2017 *Phys. Rev. Lett.* **118**(16) 164801 URL https://link.aps.org/doi/10.1103/PhysRevLett.118.164801
[25] Turnbull D, Bucht S, Davies A, Haberberger D, Kessler T, Shaw J L and Froula D H 2018 *Phys. Rev. Lett.* **120**(2) 024801 URL https://link.aps.org/doi/10.1103/PhysRevLett.120.024801
[26] Froula D H, Turnbull D, Kessler T, Haberberger D, Bahk S W, Begishev I A, Boni R, Bucht S, Davies A, Katz J and Shaw J L 2018 *Nat. Phot.* **12** 262–265 URL https://www.nature.com/articles/s41566-018-0121-8
[27] Sainte-Marie A, Gobert O and Quéré F 2017 *Optica* **4** 1298–1304 URL http://www.osapublishing.org/optica/abstract.cfm?URI=optica-4-10-1298
[28] Palastro J P, Turnbull D, Bahk S W, Follett R K, Shaw J L, Haberberger D, Bromage J and Froula D H 2018 *Phys. Rev. A* **97**(3) 033835 URL https://link.aps.org/doi/10.1103/PhysRevA.97.033835
[29] Turnbull D, Franke P, Katz J, Palastro J P, Begishev I A, Boni R, Bromage J, Milder A L, Shaw J L and Froula D H 2018 *accepted to Phys. Rev. Lett.*
[30] Sprangle P, Esarey E and Krall J 1996 *Phys. Rev. E* **54**(4) 4211–4232
[31] Keldysh L V 1965 *JETP* **20** 1307–1319 ISSN 0038-5646
[32] Mori W B 1991 *Physical Review A* **44**(8) 5118–5121 URL https://link.aps.org/doi/10.1103/PhysRevA.44.5118
[33] Esarey E, Joyce G and Sprangle P 1991 *Physical Review A* **44**(6) 3908–3911 URL https://link.aps.org/doi/10.1103/PhysRevA.44.3908